J Mol Model (2001) 7:265–270
DOI 10.1007/s008940100041

ORIGINAL PAPER

Tanja Schulz · Rolf D. Schmid · Jürgen Pleiss

Structural basis of stereoselectivity in *Candida rugosa* lipase-catalyzed hydrolysis of secondary alcohols

Received: 6 April 2001 / Accepted: 6 June 2001 / Published online: 21 July 2001

Abstract Lipases are widely used catalysts for highly enantioselective resolution of chiral secondary alcohols. While stereopreference is determined predominantly by the substrate structure, stereoselectivity (enantioselectivity and diastereoselectivity) depends on the atomic details of interactions between substrate and lipase. Experimentally obtained stereoselectivity and activity in the hydrolysis of butanoic acid esters of two secondary alcohols with two neighboring stereocenters by *Candida rugosa* lipase have been investigated by computer-aided molecular modeling of tetrahedral substrate intermediates in complex with the lipase. Breakdown of these intermediates is considered to be the rate-limiting step. Steric interactions of stereoisomers with the side chain of catalytic histidine led to different orientations of the imidazole. The distance $d(H_{N\varepsilon}–O_{alc})$ between $H_{N\varepsilon}$ of the imidazole side chain of catalytic histidine and the alcohol oxygen of the substrate was identified to correlate with the experimentally determined reactivity order of the four stereoisomers. Modeled distances $d(H_{N\varepsilon}–O_{alc})$ were short (=1.8 Å) for *RR* stereoisomers, which were also found to be hydrolyzed most rapidly experimentally; distances $d(H_{N\varepsilon}–O_{alc})$ were about 2 Å for *SS* and *SR* stereoisomers, which were converted at similar rates but at a lower rate than *RR* stereoisomers; finally, distances $d(H_{N\varepsilon}–O_{alc})$ for *SR* stereoisomers were greater than 4 Å, in accordance with very slow conversion of *SR* stereoisomers.

Keywords *Candida rugosa* lipase · Enantioselectivity · Diastereoselectivity · Molecular modeling · Secondary alcohol

T. Schulz · R.D. Schmid · J. Pleiss (✉)
Institute of Technical Biochemistry,
University of Stuttgart, Allmandring 31,
70569 Stuttgart, Germany
e-mail: Juergen.Pleiss@po.uni-stuttgart.de
Tel.: +49-711-685-3191, Fax: +49-711-685-3196

Introduction

There has been growing interest among organic chemists in using biotransformations to prepare enantiomerically pure chemicals. A widely employed class of hydrolytic enzymes are lipases (EC 3.1.1.3) because of their high enantioselectivity, activity and stability, and their broad substrate specificity. [1] Chiral secondary alcohols are a well-investigated class of substrates, [2] which are converted in lipase-catalyzed kinetic resolution through hydrolysis, esterification and transesterification. The stereopreference of most secondary alcohols can be predicted by a general rule, [3] which has been validated experimentally. The rule (Fig. 1a) assumes that enantiomeric discrimination of lipases is predominantly based on the relative size of substituents at the stereocenter (α-selectivity).

Recently, the influence of β-selectivity toward secondary alcohols with two neighboring stereocenters, which contain an additional stereocenter at the β carbon (Fig. 1b), has been investigated experimentally. [4] Enantio- and diastereoselectivities in the *C. rugosa* lipase-catalyzed hydrolysis of the four stereoisomers of acetic acid esters of **1** and **2** were measured, [4] and the reactiv-

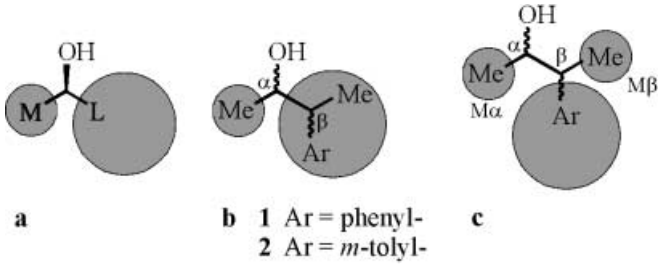

Fig. 1 **a** An empirical rule to predict the configuration of the fast-reacting enantiomer of chiral secondary alcohols in lipase-catalyzed conversions; [3] M, medium-sized substituent (e.g. methyl); L, large substituent (e.g. phenyl). **b** Classification of large and medium-sized substituents of secondary alcohols with two neighboring stereocenters **1** and **2** in accordance to (a); stereocenters are labeled α and β. **c** Classification of medium-sized substituents Mα and Mβ at stereocenters α and β, respectively, and large substituent (e.g. Ar) at the β stereocenter

ity pattern of the four isomers was determined: the *RR* isomer was hydrolyzed most rapidly, followed by *SS* and *RS*, and finally by the *SR* isomer. The two substrates have the same reactivity pattern and diastereoselectivity, while substrate **2** has decreased enantioselectivity.

The rule (Fig. 1a) for predicting the stereopreference of secondary alcohols assumes that fast conversion depends on the configuration at the α-stereocenter. Therefore, one would expect stereoisomers with the preferred configuration at the α-position – the *RR* and the *RS* stereoisomers for substrates **1** and **2** – to be hydrolyzed more rapidly than stereoisomers *SS* and *SR*. However, it has been shown experimentally that *RS* hydrolyzes slightly more slowly than *SS* stereoisomers. Therefore, the rule does not hold for stereoisomers of secondary alcohols with two neighboring stereocenters. Since classification of substituents according to this rule is not appropriate for substrates **1** and **2**, a different classification of substituents must be considered (Fig. 1c). The rule holds, however, for each enantiomeric pair separately, and predicts the stereopreference correctly: *RR* is preferred over *SS*, *RS* is preferred over *SR*. While stereopreference is successfully predicted by the rule, reaction rates of stereoisomers and the quantitative degree of stereoselectivity – enantio- and diastereoselectivity – could not be predicted.

We have reported [5] a simple model that allows prediction of the enantioselectivity of *Pseudomonas cepacia* lipase-catalyzed conversion of secondary alcohols. The model is based on a single geometrical parameter of tetrahedral substrate–lipase intermediates of slow-reacting enantiomers – the distance $d(H_{N\varepsilon}–O_{alc})$ between the hydrogen atom $H_{N\varepsilon}$ of catalytic histidine and the alcohol oxygen of the substrate. Quantum chemical methods [6] have identified the transfer of the hydrogen atom $H_{N\varepsilon}$ from catalytic histidine to the alcohol oxygen of the substrate and the breakdown of the tetrahedral intermediate as the rate-limiting step in lipase-catalyzed hydrolysis. [7, 8] As short distances $d(H_{N\varepsilon}–O_{alc})$ are indicative of fast conversion, short distances $d(H_{N\varepsilon}–O_{alc})\leq 2.0$ Å in complexes of the slow-reacting enantiomer correlate with low enantioselectivity, while large distances $d(H_{N\varepsilon}–O_{alc})\geq 2.2$ Å are observed for substrates that are converted at high enantioselectivity.

In this study, we have extended the model to predict β-selectivity in the hydrolysis of butanoic acid esters of secondary alcohols with two neighboring stereocenters and transferred the model to a different lipase, that from *C. rugosa*. Based on experimentally determined data of *C. rugosa* lipase-catalyzed hydrolyses of substrates **1** and **2**, the relevance of $d(H_{N\varepsilon}–O_{alc})$ for the prediction of stereoselectivity was verified.

Methods

Hard- and software

Molecular modeling studies were carried out on Silicon Graphics workstations Indigo2/R10000. The software for energy minimization and molecular dynamics simulations was Sybyl 6.3 and Sybyl 6.5 (Tripos, St. Louis, MO) using the Tripos force field. [9]

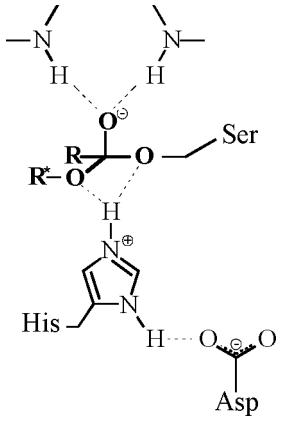

Fig. 2 Simplified binding site model of substrate–lipase complexes, including catalytically important residues and residues of the oxyanion-hole, and the first tetrahedral intermediate in lipase-catalyzed hydrolysis of secondary alcohols. The substrate is shown in bold; R, fatty acid chain; R* chiral alcohol moiety

Molecular modeling

The X-ray structure of the open conformation of inhibited *C. rugosa* lipase [10] in complex with (1*R*)-menthyl-hexyl phosphonate [11] was taken from the PDB [12] (entry 1LPO). Solvent molecules and the inhibitor were removed and butanoic acid esters of the four stereoisomers of substrates **1** and **2** were covalently docked in their tetrahedral intermediate structure (Fig.2). Docking was guided by the substrate-analogous inhibitor (1*R*)-menthyl-hexyl phosphonate. [11] The oxyanion was oriented toward the oxyanion hole, and the tetrahedral carbon of the substrate was covalently linked to the side chain oxygen Oγ of catalytic serine; thus, the substrate–lipase complex mimics the first transition state in lipase-catalyzed hydrolysis of esters of secondary alcohols. The protonation state at the catalytic histidine and the partial charges of the catalytic serine, histidine and substrate were modified [13] as calculated by the semi-empirical method MNDO94/PM3. [14] The structures of the substrate–lipase complexes were refined by energy minimization, and subsequent molecular dynamics simulations in vacuo with constrained protein backbone were performed. [5] The substrate–lipase complexes were equilibrated in three intervals of 1 ps at 5 K, 30 K and 70 K, and 4 ps at 100 K, followed by a production phase of 1 ps at 100 K. The step size was 1 fs up to 30 K and 0.5 fs for 70 and 100 K. The non-bonded interaction cut-off was set to 8 Å, the coupling constant to 10 fs, and the dielectric constant to 1.0. Conformers were saved every 40 fs. An average structure was created by superimposing and averaging 25 substrate–lipase complex structures of the production phase. The results of averaged struc-

tures from simulations at 100 K were analyzed by measuring the catalytically important distance $d(H_{N\varepsilon}–O_{alc})$.

Results

Binding of substrates

Secondary alcohols **1** and **2** have two substituents of different size at the α stereocenter. For both substrates, the medium-sized substituent at the α stereocenter is methyl (Mα). The large substituent at the α stereocenter includes the β stereocenter; substituents at the β stereocenter are classified as medium-sized (Mβ) and large substituents (L). Mβ is methyl for **1** and **2**, L is phenyl or *m*-tolyl for **1** or **2**, respectively (Fig. 1c).

Two spherical binding pockets – BPα and BPβ – were identified (Fig.3), which have an appropriate geometry for binding medium-sized substituents Mα and Mβ of **1** and **2**. The binding site of *C. rugosa* lipase is further limited by two rigid *stops* composed of backbone atoms, which are situated above and below the two stereocenters.

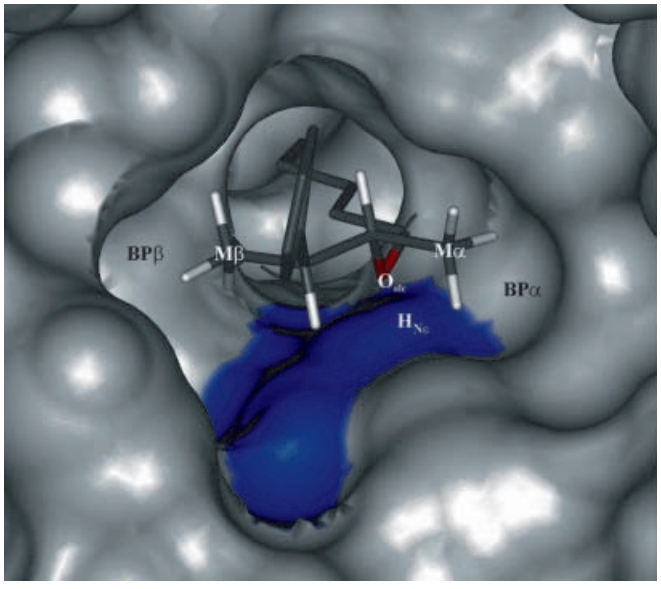

Fig. 3 Three-dimensional binding site model of the lipase from *C. rugosa* in complex with the stereoisomer *RR*-**1**. The two spherical binding pockets are labelled BPα and BPβ; medium-sized substituents of *RR*-**1** are labeled Mα and Mβ; the surface of side chain imidazole of catalytic histidine is colored in *blue*, and the positions of $H_{N\varepsilon}$ and O_{alc} are indicated. Hydrogen atoms at Mα and Mβ and at the stereocenters α and β are displayed and colored *white*; carbon atoms are colored *gray*, the alcohol oxygen O_{alc} is colored *red*; hydrogen atoms of the large substituent and the fatty acid chain are undisplayed

For enantiomers *RR* and *SS* of both substrates, Mα and Mβ bind to BPα and BPβ, respectively, and the hydrogen atoms at the stereocenters are directed toward the rigid *stops* (Fig. 4a). Thus, both enantiomers have minimal repulsive interactions and are well stabilized. During molecular dynamics simulations, no major conformational changes occurred. For both substrates, complexation of the most rapidly converted stereoisomer *RR* results in a proper orientation of the side chain imidazole of the catalytic histidine, which is a prerequisite for efficient catalysis. Slower conversion of the *SS* isomer is due to a slight change in the orientation of the side chain imidazole of the catalytic histidine. This difference in side chain orientation results from different steric interactions of the active histidine with substituents at the α stereocenter of the *RR* and *SS* enantiomers, which is caused by the inversion at the two stereocenters.

For both enantiomers of the enantiomeric pair *RS* and *SR*, Mα binds to BPα, and the hydrogen atom at the β stereocenter is directed toward BPβ. Repulsive interactions of Mβ with either of two rigid *stops* occur. During molecular dynamics simulations, both stereoisomers show geometric fluctuations. Mβ of the *RS* isomer interacts with a *stop* composed of backbone atoms including the catalytic histidine, and pushes the side chain imidazole away from its proper orientation. Strong steric repulsion with backbone atoms of the residues forming BPβ occurs for the *SR* isomers, and results in a complete reorientation of the substrates during the simulations. In

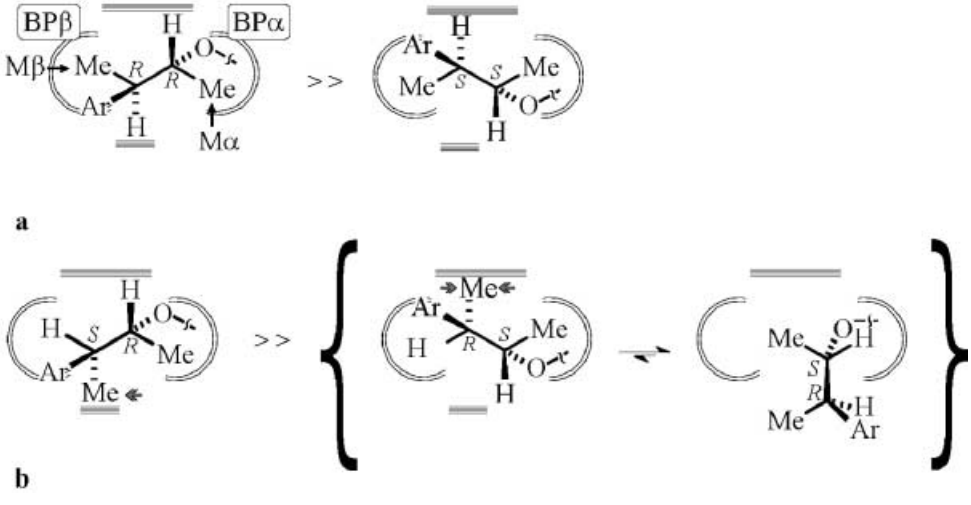

Fig. 4a,b Orientation of the four stereoisomers, *RR*, *SS*, *RS* and *SR*, in the binding site of *C. rugosa* lipase: orientation of **a** the enantiomeric pair *RR*-**1/2** and *SS*-**1/2** and **b** of the second enantiomeric pair *RS*-**1/2** and *SR*-**1/2** as well as the reoriented conformation of *SR*-**1/2** in the binding site of *C. rugosa* lipase.Arrows shaded in *gray* indicate repulsive steric interactions; rigid *stops* (≡) and binding pockets BPα and BPβ of the lipase are indicated; –Ar represents phenyl or *m*-tolyl.

Table 1 Experimental substrate ranking and enantioselectivities; experimental diastereoselectivities are 66% for **1** and 65% for **2**; the calculated distances $d(H_{N\varepsilon}–O_{alc})$ of tetrahedral substrate–lipase intermediates in asymmetric enzymatic hydrolysis of the four stereoisomers of substrates **1** and **2** with *C. rugosa* lipase

Experimental substrate ranking	Configuration (α, β)	**1**		**2**	
		exp. e.e. (%)	$d(H_{N\varepsilon}–O_{alc})$ (Å)	exp. e.e. (%)	$d(H_{N\varepsilon}–O_{alc})$ (Å)
1	*R*,*R*	62	1.7	35	1.8
2	*S*,*S*		2.0		2.0
3	*R*,*S*	59	2.1	43	2.0
4	*S*,*R*		4.3		4.1

the reoriented conformation (Fig. 4b), the hydrogen atom at the α stereocenter is directed toward BPα, and Mα toward BPβ without binding to it. Repulsive steric interactions of the substituents at the β stereocenter occur. In addition, in this conformation the substrate showed large motions during the simulations, and pushed away the side chain imidazole of the catalytic histidine from its productive orientation.

Ranking by $d(H_{N\varepsilon}–O_{alc})$

To quantify these visual observations, the catalytically important distance $d(H_{N\varepsilon}–O_{alc})$ of the four stereoisomers was measured (Table 1) and compared with experimentally determined data. The *RR* isomers had the shortest distance (1.7 Å and 1.8 Å for **1** and **2**, respectively), which correlates with experimentally observed reaction rates. The distances for *SS* and *RS* stereoisomers were similar (2.0 Å for *SS*-**1**/**2** and *RS*-**2**, 2.1 Å for *RS*-**1**), which correlates to similar rates of conversion. Distances for *SR* stereoisomers of **1** and **2** were $d(H_{N\varepsilon}–O_{alc})$>4 Å, thus preventing the formation of a hydrogen bond between Nε and O_{alc}. This correlates with very slow conversion of *SR* stereoisomers. Thus, ranking of the four stereoisomers by the modeled distance $d(H_{N\varepsilon}–O_{alc})$ correlates to experimentally determined reactivity orders of substrates **1** and **2**.

Activity of substrates **1** and **2**

Experimentally determined catalytic activity is in accordance with short distances $d(H_{N\varepsilon}–O_{alc})$ of the experimentally most rapidly converted stereoisomers, which is isomer *RR* for substrates **1** and **2**. Since the modeled distance $d(H_{N\varepsilon}–O_{alc})$ was slightly smaller for substrate **1** than for substrate **2**, substrate **1** was predicted to be converted at a higher rate. For a correct prediction of activity, all highly populated substrate conformations in the lipase binding site must be considered. Two different orientations were observed for substrate **2**: the *m*-methyl group at the tolyl substituent was situated at either of the two *meta*-positions. However, one of the two orientations of the *RR* stereoisomer resulted in a non-productive hydrogen bond pattern (data not shown). Thus, both the shorter distance of *RR*-**1** and the population of two different conformations by *RR*-**2** – one with an active and one with a non-active hydrogen bond pattern – predict higher lipase activity toward substrate **1**, which is in accordance with experiment. Different orientations of *meta* substituents in isomers *SS*, *RS* and *SR* of substrate **2** were also investigated, but did not influence the distances $d(H_{N\varepsilon}–O_{alc})$ for *SS*-**2** and *RS*-**2**. For *SR*-**2**, only one orientation with a non-active hydrogen bond pattern was identified.

Enantioselectivity

Enantioselectivity is based on the ratio between lipase activity toward fast-reacting and slow-reacting enantiomers $[E=(k_{cat}/K_m)_{fast}/(k_{cat}/K_m)_{slow}]$. Thus, high enantioselectivity results from large differences in activity, which should be reflected in large differences of $d(H_{N\varepsilon}–O_{alc})$ between fast- and slow-reacting enantiomers.

For the enantiomeric pair *RR* and *SS*, the differences $\Delta d(H_{N\varepsilon}–O_{alc})=d(H_{N\varepsilon}–O_{alc})^{RR}–d(H_{N\varepsilon}–O_{alc})^{SS}$ are 0.3 Å and 0.2 Å for substrate **1** and **2**, respectively. The larger difference $\Delta d(H_{N\varepsilon}–O_{alc})$ for substrate **1** corresponds to a higher enantiomeric excess for *RR*/*SS*-**1** (e.e. 62%) than for *RR*/*SS*-**2** (e.e. 35%).

For the enantiomeric pair *RS* and *SR*, the difference $\Delta d(H_{N\varepsilon}–O_{alc})$ is 2.2 Å and 2.1 Å for substrate **1** and **2**, respectively. This agrees with the experimentally determined slightly higher enantiomeric excess for *RS*/*SR*-**1** (e.e. 59%) than for *RS*/*SR*-**2** (e.e. 43%).

Diastereoselectivity

Diastereoselectivity was estimated by the ratio of distances $d(H_{N\varepsilon}–O_{alc})$ between enantiomeric pairs $([d(H_{N\varepsilon}–O_{alc})_{RR}+d(H_{N\varepsilon}–O_{alc})_{SS}]/[d(H_{N\varepsilon}–O_{alc})_{RS}+d(H_{N\varepsilon}–O_{alc})_{SR}])$. This ratio was determined as 0.6 for both substrates, thus indicating similar diastereoselectivities. The prediction of the model agreed with experimentally determined diastereoselectivities of 66% for **1** and 65% for **2**.

Discussion

The geometrical parameter $d(H_{N\varepsilon}–O_{alc})$ allows substrate ranking and a qualitative interpretation of experimentally

determined activities of *C. rugosa* lipase toward substrates **1** and **2,** and modeling of relative enantio- and diastereoselectivities of the two substrates.

Prediction of stereopreference

Stereopreference toward chiral secondary alcohols has been predicted reliably by an empirical rule (Fig. 1a), which assumes that enantiomeric discrimination is predominantly based on the structure of the secondary alcohol moiety [3] (α-selectivity). The rule also holds for secondary alcohols with two neighboring stereocenters **1** and **2**, if stereopreference is predicted for each enantiomeric pair separately. However, the rule provides no information about stereopreference and reaction rates of the four stereoisomers (ranking), and enantio- and diastereoselectivity are not predicted. Thus, to gain insight into atomic details of interactions which mediate stereopreference, reaction rates, enantio- and diastereoselectivity of substrates **1** and **2** (α- and β-selectivity), it is not sufficient to consider only structural properties of the substrate, but also interactions between the binding site of the biocatalyst and the substrates must be considered within the model. Therefore, we investigated the first tetrahedral intermediates in the lipase-catalyzed hydrolysis of **1** and **2**, since the breakdown of this intermediate is considered to be the rate-limiting step in lipase-catalyzed hydrolysis. [6]

Docking

Alcohol moieties include several rotatable bonds (degrees of freedom), and therefore the conformational space of the alcohol moiety is large. However, flexibility is restricted due to two well-defined binding pockets of the substrate binding site: the hydrophobic tunnel, which accommodates the butanoic acid chain; Mα and Mβ, which bind the medium-sized substituents at the α and β stereocenter; two rigid *stops*, which consist of backbone atoms and limit the size of the binding site.

Comparison of X-ray structures (open conformations) of free [15] (PDB entry 1crl) and inhibited *C. rugosa* lipase [12] (PDB entry 1lpm) has shown that backbone atoms hardly move upon substrate binding (Cα r.m.s. 0.2 Å), and thus follow the lock and key model, [16] while side chains reorientate and show induced fit behavior. [17] Accordingly, we performed molecular dynamics simulations by constraining the position of the backbone atoms and allowing the side chains and the substrate to move.

Tetrahedral intermediates of stereoisomers differed in the orientation of substituents in the binding site of *C. rugosa* lipase, resulting in different steric and physicochemical substrate–lipase interactions and therefore differences in the distance $d(H_{N\varepsilon}–O_{alc})$. The high flexibility of side chain imidazole of the catalytic histidine is in accordance with X-ray structures of inhibited *C. rugosa* lipase complexed with either enantiomer of menthyl hexylphosphonate, [12] and with our model for *P. cepacia* lipase, [5] where slow-reacting enantiomers in both cases distorted the orientation of the imidazole ring of the catalytic histidine and broke the hydrogen bond between imidazole and the oxygen of the alcohol oxygen of the substrate, thus preventing efficient catalysis of slow-reacting enantiomers and promoting high enantioselectivity.

Prediction of activity and stereoselectivity (enantio- and diastereoselectivity)

Quantum chemical methods [18, 19] have identified the first tetrahedral substrate–lipase complex and the distance $d(H_{N\varepsilon}–O_{alc})$ as a critical parameter of catalytic activity. Since differences of lipase activity [20, 21] toward two enantiomers and diastereomers result in experimentally observable enantioselectivity $[E=(k_{cat}/K_m)_{fast}/(k_{cat}/K_m)_{slow}]$ and diastereoselectivity $([(k_{cat}/K_m)_{RR}+(k_{cat}/K_m)_{SS}]/[(k_{cat}/K_m)_{RS}+(k_{cat}/K_m)_{SR}])$, respectively, the hydrogen-bonding network, [6] especially the distance $d(H_{N\varepsilon}–O_{alc})$, is expected to be relevant to activity and stereoselectivity.

Distances $d(H_{N\varepsilon}–O_{alc})$ of stereoisomers of **1** and **2** showed a correct substrate ranking and therefore a correct prediction of activity of fast- and slow-reacting stereoisomers. However, comparison of different substrates through kinetic studies [6] has demonstrated that differences in the conversion of enantiomers do not result from enhanced reactivity of fast-reacting enantiomers but from reduced reactivity of slow-reacting enantiomers. Thus, the distance of the fast-reacting stereoisomers (considering enantiomeric pairs) *RR* and *RS* should be of less importance with regard to stereoselectivity. This is true for the enantiomeric pair *RS*–*SR*, where the distance $d(H_{N\varepsilon}–O_{alc})$ is larger for stereoisomer *SR*-**1** than for *SR*-**2**, resulting in higher enantioselectivity of substrate **1**. For the enantiomeric pair *RR*–*SS* of substrates **1** and **2**, slow-reacting enantiomers (*SS*-**1**/**2**) show the same distance $d(H_{N\varepsilon}–O_{alc})$; however, substrate **1** shows higher enantioselectivity. This is due to a second highly populated binding mode of *RR*-**2**, caused by the *meta*-methyl group of the large substituent, which shows a non-productive hydrogen bond pattern and therefore reduced activity of *RR*-**2**. The distance $d(H_{N\varepsilon}–O_{alc})$ is an appropriate geometrical parameter to reproduce experimentally determined activity and relative enantio- and diastereoselectivity in *C. rugosa* lipase-catalyzed conversion of **1** and **2**.

The model

The model is based on structural properties of the first tetrahedral intermediate in the lipase-catalyzed hydrolysis of the butanoic acid ester of **1** and **2**. As shown previously, docking methods are generally reliable and able to predict stereopreference correctly. [5, 22, 23] However, problems occur when energy-based scoring strategies are

used to rank substrates. [24] To circumvent these limitations, our model uses common docking methods, while ranking is based on a new approach, a geometry-based scoring strategy.

Solvent can contribute significantly to activity and selectivity, but solvent engineering studies have shown that finding the best organic solvent for a lipase-catalyzed resolution is still a trial and error process, since there is no general rule to predict the best organic solvent. Our simulations of tetrahedral intermediates were performed in vacuo, and solvent effects were completely neglected. This model has previously been applied to *P. cepacia* lipase, [5] where we observed a good correlation of the distance $d(H_{N\varepsilon}–O_{alc})$ to most solvent-optimized enantioselectivities. It seems that the maximum enantioselectivity that can be attained by solvent engineering is limited by the structure of biocatalyst and substrate. If this "structure-based enantioselectivity" is high and the optimal solvent is used, the two enantiomers are well separated by the lipase, while using sub-optimal solvent decreases enantioselectivity. However, if the "structure-based enantioselectivity" is low, solvent engineering is not expected to be able to increase enantioselectivity.

This extension of our previous model, developed to investigate enantioselectivity of *P. cepacia* lipase toward chiral secondary alcohols, [5] demonstrates that the model is transferable to different lipases as well as to different classes of substrates. The relevance of the distance $d(H_{N\varepsilon}–O_{alc})$ for predicting activity and stereoselectivity was verified. Further experimental data of lipase-catalyzed conversion of chiral secondary alcohols and other substrate classes will improve the model. Generalizing it to other lipases will help to understand common stereoselectivity-mediating factors and facilitate protein engineering studies.

References

1. Schmid RD, Verger R (1998) Angew Chem Int Ed Engl 37: 1608–1633
2. Kazlauskas RJ, Bornscheuer UT (1998) Biotransformations with Lipases. In: Rehm HJ, Reed G, Pühler A, Stadler PJW, Kelly DR (eds) Biotechnology, Vol. 8a. Wiley-VCH, Weinheim, pp 37–191
3. Kazlauskas RJ, Weissfloch ANE, Rappaport AT, Cuccia L (1991) J Org Chem 56:2656–2665
4. Angelis YS, Smonou I (1998) Tetrahedron Lett 39:2823–2826
5. Schulz T, Pleiss J, Schmid RD (2000) Protein Sci 9:1053–1062
6. Ema T, Kobayashi J, Maeno S, Sakai T, Utaka M (1998) Bull Chem Soc Jpn 71:443–453
7. Chapus C, Sémériva M, Bovier-Lapierre C, Desnuelle P (1976) Biochemistry 15:4980–4987
8. Chapus C, Sémériva M (1976) Biochemistry 15:4988–4991
9. Clark M, Cramer RD III, van Opdenbosch N (1989) J Comput Chem 10:982–1012
10. Grochulski P, Young L, Schrag JD, Cygler M (1994) Protein Sci 3:82–91
11. Cygler M, Grochulski P, Kazlauskas RJ, Schrag JD, Bouthillier F, Rubin B, Serreqi AN, Gupta AK (1994) J Am Chem Soc 116:3180–3186
12. Bernstein FC, Koetzle TF, Williams GJB, Meyer EF Jr, Brice MD, Rodgers JR, Kennard O, Shimanouchi T, Tasumi M (1977) J Mol Biol 112:535–542
13. Holzwarth HC, Pleiss J, Schmid RD (1997) J Mol Catal B: Enzymatic 3:73–82
14. Stewart JJP (1989) J Comput Chem 10:209–220
15. Grochulski P, Li Y, Schrag JD, Bouthillier F, Smith P, Harrison D, Rubin B, Cygler M (1993) J Biol Chem 268:12843–12847
16. Fischer E (1894) Ber Dtsch Chem Ges 27:2985–2993
17. Koshland DE, Thoma JA (1960) J Am Chem Soc 82:3329–3333
18. Hu CH, Brinck T, Hult K (1998) Int J Quantum Chem 69: 89–103
19. Monecke P, Friedemann R, Naumann S, Csuk R (1998) J Mol Model 4:395–404
20. Nakamura K, Kawasaki M, Ohno A (1996) Bull Chem Soc Jpn 69:1079–1085
21. Nishizawa K, Ohgami Y, Matsuo N, Kisida H, Hirohara H (1997) J Chem Soc, Perkin Trans 2:1293–1298
22. Scheib H, Pleiss J, Schmid RD (1998) Protein Eng 11:675–682
23. Scheib H, Pleiss J, Kovac A, Paltauf F, Schmid RD (1999) Protein Sci 8:215–221
24. Haeffner F, Norin T, Hult K (1998) Biophys J 74:1251–1262